Int. J. Heat Mass Transfer. Vol. 35, No. 1, pp. 63–72, 1992
Printed in Great Britain

0017-9310/92 $5.00 + 0.00


# Direct-contact heat transfer to a spherical-cap liquid/vapor two-phase bubble

YASUHIKO H. MORI and NOBUO EHARA
Department of Mechanical Engineering, Keio University, 3-14-1 Hiyoshi, Kohoku-ku, Yokohama 223, Japan

(*Received* 18 *December* 1990 *and in final form* 6 *March* 1991)

**Abstract**—The heat transfer to spherical-cap bubbles, each consisting of a growing vapor phase and a reducing yet-to-be vaporized liquid phase, is considered. The liquid phase is supposed to form, in each bubble, a bottom layer supported by the flat base of the bubble, while the rest is occupied by the heat insulating vapor phase. The heat transfer causing the evaporation is thus assumed to occur exclusively at the rear of the bubble covered with a wake. Predictions of quasi-steady, overall heat transfer are made and compared with relevant experimental results.

## 1. INTRODUCTION

IN THE course of evaporation of a liquid drop in an immiscible liquid, a 'two-phase bubble' consisting of a growing vapor phase and a reducing liquid phase is evolved from the drop. The two-phase bubble changes its shape from nearly spherical to oblate ellipsoidal, and probably to spherical cap [1] so far as the continuous phase is of a not-too-viscous liquid such as water or brine—a situation encountered in various engineering applications such as direct-contact boilers for power plant use, slush-ice cool storage facilities, etc. The larger the drop set to evaporate is, the relatively earlier in the whole evaporation process the two-phase bubble will attain the spherical-cap shape. In this paper we are concerned with the heat transfer to each two-phase bubble that has attained the spherical-cap shape.

A number of studies have been performed on single-phase spherical-cap bubbles as reviewed by Wegener and Parlange [2] and Clift *et al.* [3], and it has been established that the spherical-cap shape prevails when $Eo > 40$, where $Eo$ is the Eötvös number defined as

$$Eo = \Delta\rho g D^2/\sigma. \quad (1)$$

Here we assume that the same rule is applicable to the shape of two-phase bubbles provided that we substitute the interfacial tension at the 'vapor/continuous phase' boundary for $\sigma$ and the difference between $\rho_c$, the density of the continuous phase, and the mean density of the bubble for $\Delta\rho$. Figure 1 shows the dependencies, on the drop diameter $D_0$ and on the pressure $p_\infty$, of the mass fraction of vapor in each bubble, $\xi$, satisfying the condition that $Eo = 40$. In the case of n-pentane drops evaporating in water as exemplified here, we note that the spherical-cap can be the basic shape of each bubble through a significant portion of its evaporation process whenever $D_0$ is as large as several millimeters and $p_\infty$ is no more than several atmospheres.

In spite of its practical importance observed in the above example, little has been clarified about the heat transfer to spherical-cap-shaped two-phase bubbles. Klipstein [1] considered that each spherical-cap bubble has a dimpled bottom, which supports an annular pool of the yet-to-be vaporized liquid, and that the heat transfer across the liquid/liquid interface at the bottom of the bubble is the major portion of the total heat transfer to the 'vapor/yet-to-be vaporized liquid' interface, i.e. the vapor-generating interface inside the bubble. Later Simpson *et al.* [4] presented an analytic study of heat transfer to a cylindrical-cap bubble—a two-dimensional analog of a spherical-cap bubble—based on a completely different modeling of the behavior of the yet-to-be vaporized liquid inside the bubble. They assumed that the oscillation of the bubble related to the wake shedding causes the yet-to-be vaporized liquid inside the bubble to slosh from side to side, forming a thin film spread over the front surface of the bubble. The heat transfer across the continuous-phase-side boundary layer over the front surface and then across the film of the yet-to-be vaporized liquid is considered. Comparing the results thus deduced analytically with those of experiments with butane drops evaporating in water or an aqueous solution of sodium chloride, Simpson *et al.* determined the effective thickness of the film of the yet-to-be vaporized liquid and reached a conclusion that the film provides the major resistance against the heat transfer to the 'vapor/yet-to-be vaporized liquid' interface.

The theoretical approach of Simpson *et al.* [4] is quite original and, in our opinion, debatable. The validity of the assumption of the thin liquid-film formation over the bubble surface is solely supported by the agreement, between their theoretical predictions and their own experimental results, in the tendency of

## NOMENCLATURE

$A$ whole surface area of bubble
$A_e$ surface area of sphere volume-equivalent to bubble
$A_r$ base area of bubble
$b$ width of bubble
$c_p$ specific heat capacity
$D$ diameter of sphere volume-equivalent to bubble
$Eo$ Eötvös number defined in equation (1)
$f$ frequency of vortex shedding from wake
$Fr$ Froude number, $U^2/gD$
$g$ acceleration due to gravity
$G_w$ geometrical parameter defined in equation (6)
$H$ vertical distance travelled by bubble
$h_{lv}$ latent heat of vaporization of the dispersed-phase substance
$H_m$ one-half the height of the continuous phase above the elevation where evaporation starts
$K$ overall heat transfer coefficient averaged over $A_r$
$m$ exponent of cosine in equation (25)
$n$ exponent of $s$ in equation (25)
$Nu$ Nusselt number, $\alpha D/\lambda_c$
$p_\infty$ static pressure in the continuous phase
$Pe$ Péclet number, $UD/\kappa_c$
$Pr$ Prandtl number, $\nu_c/\kappa_c$
$Q$ heat transferred to bubble after the initiation of evaporation
$r$ radial distance measured from bubble axis
$r_l$ $r$ at the outer edge of axisymmetrically-spread yet-to-be vaporized liquid
$R_c$ radius of curvature at bubble front
$Re$ Reynolds number, $UD/\nu_c$
$s$ fraction of $A_r\zeta$ wherein the local thickness of yet-to-be vaporized liquid is larger than, or equal to, a particular value of $\delta$
$Sr$ Strouhal number, $fb/U$
$t$ time lapse after the initiation of evaporation
$T_s$ temperature at the liquid/vapor interface inside bubble, which is assumed, in experimental-data processing, to be the temperature at which $p_\infty$ is equal to the saturated vapor pressure of the dispersed-phase substance plus, if not negligibly small, that of the continuous-phase substance; should be in Kelvins in equations (A4)–(A6)
$\Delta T$ difference between undisturbed temperature in the continuous phase and $T_s$
$U$ rise velocity of bubble
$V$ volume of bubble
$V^*$ wake-to-bubble volume ratio.

Greek symbols

$\alpha$ continuous-phase-side heat transfer coefficient based on $A_e$
$\alpha_{ov}$ overall heat transfer coefficient based on $A_e$
$\alpha_r$ continuous-phase-side heat transfer coefficient at the bubble rear
$\Gamma$ constant used in equation (14)
$\delta$ local thickness of yet-to-be vaporized liquid
$\delta_{cr}$ critical value of $\delta$ for the onset of dry-patch growth in the layer of yet-to-be vaporized liquid
$\delta_{max}$ maximum of $\delta$
$\bar{\delta}$ $\delta$ averaged over $A_r$
$\bar{\delta}_l$ $\delta$ averaged over $A_r\zeta$
$\zeta$ fraction of $A_r$ covered with yet-to-be vaporized liquid
$\theta_w$ polar angle at the bubble rim
$\kappa$ thermal diffusivity
$\lambda$ thermal conductivity
$\nu$ kinematic viscosity
$\xi$ mass fraction of vapor in bubble
$\rho$ mass density
$\sigma$ 'vapor/continuous-phase liquid' interfacial tension
$\chi$ ratio of dissipation rate by turbulent motion to the total energy dissipation rate
$\psi$ constant indicating the ratio of $(\bar{\delta}_l-\bar{\delta})$ to $(\delta_{cr}-\bar{\delta})$.

Subscripts

c continuous-phase liquid
dl dispersed-phase substance in the state of saturated liquid
dv dispersed-phase substance in the state of saturated vapor
m mean value in the continuous phase or local value at $H = H_m$
0 initial condition before the onset of evaporation.

the instantaneous heat transfer coefficient to increase with progress of evaporation. However, such a tendency is not necessarily supported by the other experimental results reported so far. In fact, the experiments of Sideman and Taitel [5] and those in our laboratory [6] show such a tendency that the instantaneous heat transfer coefficient decreases with progress of evaporation over the major portion of each evaporation

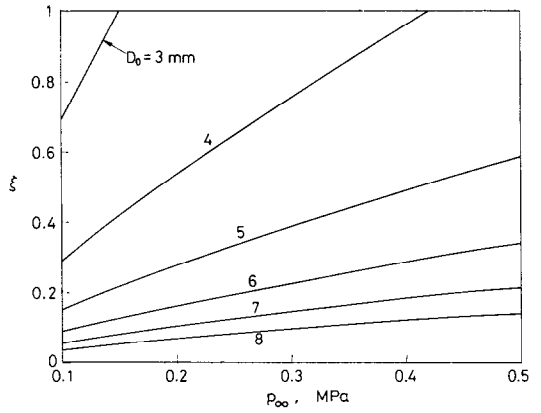


FIG. 1. Vapor mass fraction yielding the minimal Eötvös number, $Eo = 40$, for the possible deformation of n-pentane two-phase bubbles in water into spherical caps.

process. Another debatable question is that the tendency indicated by the experiments by Simpson *et al.* might also be simulated on the basis of a theoretical model greatly different from their film-formation model.

In this paper, we present an analytic model which may be viewed as the reverse of the model of Simpson *et al.* We assume that the yet-to-be vaporized liquid inside a spherical-cap bubble wholly accumulates on its flat base. Consequently, the effective heat transfer area is the rear surface of the bubble that is totally covered with a wake. (In this respect, the present model constitutes a counterpart of another model that we recently developed to simulate the heat transfer through a wake behind a spherical two-phase bubble [7].) The predictions deduced from the present model are compared with relevant experimental results to evaluate to what extent the wake-region contributes to the heat transfer in real evaporation processes.

## 2. SPECIFICATIONS OF ANALYTIC MODEL

Figure 2 illustrates the two-phase bubble model outlined above. The model approximates each bubble as a segment of a sphere, with a flat base, facing a steady, uniform flow normal to the base. Flow separation from the bubble invariably occurs at its rim, thus forming a wake extending over the full width of the bubble, $b$. The separation angle $\theta_w$ is held constant during evaporation. In later calculations we exclusively assume that $\theta_w = 50°$, which is accepted as a good approximation for ordinary gas bubbles whenever $Eo \geqslant 40$ and $Re \geqslant 150$ [3]. The yet-to-be vaporized liquid forms a layer spreading over the base of each bubble. The thickness of the layer may be spatially uneven at each instant and, at each location, it may fluctuate with time because of a distortion of the nominally-flat bubble base responding to vortex shedding from the wake and/or to some turbulence inside the wake. (It is assumed that the distortion of the bubble base gives no more than a negligible effect on geometrical parameters characterizing the bubble: i.e. $b$, $R_c$, $\theta_w$ and $V$, the volume of the bubble.) Heat is transferred from the external flow to the wake and then to the liquid/liquid interface at the bubble base, from where it is conducted across the yet-to-be vaporized liquid layer to its opposite surface contacting with the vapor. No heat flow through the front spherical surface of the bubble is considered.

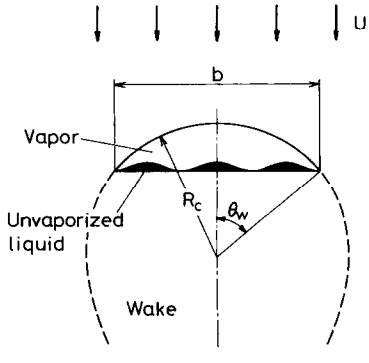


FIG. 2. Spherical-cap bubble containing yet-to-be vaporized liquid on its nominally flat base.

In calculations given in subsequent sections we necessarily use some geometrical relations relevant to the present bubble model. They are

$$V = \frac{1}{3}\pi R_c^3 G_w \tag{2}$$

$$\frac{D}{R_c} = (2G_w)^{1/3} \tag{3}$$

$$\frac{b}{D} = \frac{2\sin\theta_w}{(2G_w)^{1/3}} \tag{4}$$

$$\frac{A_r}{A_e} = \frac{\sin^2\theta_w}{(2G_w)^{1/3}} \tag{5}$$

where $D$ and $A_e$ denote the diameter and the surface area, respectively, of a sphere having the same volume as that of the bubble, $V$; $A_r$ is the area of the flat base of the bubble; and

$$G_w \equiv 2 - 3\cos\theta_w + \cos^3\theta_w. \tag{6}$$

Using equations (2) and (3) in addition to simple volume–diameter–$\xi$ relations (Appendix in ref. [7]), we can derive the following expression for $\delta$, the thickness of the yet-to-be vaporized liquid averaged over the area $A_r$ at each instant:

$$\frac{\delta}{D_0} = \frac{G_w^{2/3}}{3\sin^2\theta_w} \frac{1-\xi}{\left[1+\xi\left(\frac{\rho_{dl}}{\rho_{dv}}-1\right)\right]^{2/3}} \tag{7}$$

which is used in evaluating the internal thermal resistance, i.e. the resistance to conductive heat transfer across the layer of the yet-to-be vaporized liquid.

In the following we consider first the convective external heat transfer and then the internal and the overall heat transfer, analogously to ref. [7].

## 3. EXTERNAL HEAT TRANSFER

In this work, we do not attempt an essentially original analysis of the heat transfer to the rear of a spherical-cap bubble, but simply substitute existing solutions for the mass transfer from spherical-cap bubbles for the solution to the present problem. Two different solutions for the mass transfer are considered. The procedure of applying each of them to the present problem is explained below.

### 3.1. *Application of Weber's solution*

Weber [8] studied the mass transfer from the rear of a spherical-cap bubble on the basis of the penetration theory, assuming a characteristic contact time which is equal to the interval of the vortex shedding from the wake trailed by the bubble. He derived a solution for the time-averaged mass transfer coefficient, which can be translated into the expressions for $\alpha_r$, the heat transfer coefficient which is to prevail evenly over the area $A_r$, and for $\alpha$, the coefficient averaged over the area $A_e$, as

$$\alpha_r = \frac{2}{\sqrt{\pi}}\rho_c c_{pc} Sr^{1/2}\left(\frac{U\kappa_c}{b}\right)^{1/2} \tag{8}$$

$$\alpha = \frac{1}{2\sqrt{\pi}}\rho_c c_{pc}\left(\frac{b}{D}\right)^{3/2} Sr^{1/2}\left(\frac{U\kappa_c}{D}\right)^{1/2}. \tag{9}$$

Equation (9) can be rewritten in dimensionless form as

$$Nu = \frac{1}{2\sqrt{\pi}}\left(\frac{b}{D}\right)^{3/2} Sr^{1/2} Pe^{1/2}. \tag{10}$$

Utilizing equation (4) gives

$$Nu = \left(\frac{\sin^3\theta_w}{\pi G_w}\right)^{1/2} Sr^{1/2} Pe^{1/2}. \tag{11}$$

For further simplification, we specify $\theta_w$ and $Sr$. $\theta_w$ is set at 50° as explained before. The results of Lindt and de Groot's experiments [9] indicate that $Sr = 0.3$ is a good approximation in the range of $Re \gtrsim 2500$. With these specifications of $\theta_w$ and $Sr$ in equations (4), (6) and (11), equations (8) and (11) are rewritten respectively as

$$\alpha_r = 0.468\rho_c c_{pc}\left(\frac{U\kappa_c}{D}\right)^{1/2} \tag{12}$$

$$Nu = 0.357 Pe^{1/2}. \tag{13}$$

### 3.2. *Application of Coppus and Rietema's solution*

Coppus and Rietema [10] dealt with the same problem as the one studied by Weber [8] but with an idea that the mass transfer is controlled by the renewal of the surface at the bubble rear due to small-scale eddies in the wake. The solution they reached is rewritten for the case of heat transfer as

$$\alpha_r = \Gamma\chi^{1/4}\rho_c c_{pc}\kappa_c^{1/2}\left(\frac{gU}{V^* v_c}\right)^{1/4} \tag{14}$$

where $\Gamma$ designates a constant that originally means a proportional factor between $\alpha_r/(\rho_c c_{pc})$ (the equivalent of mass transfer coefficient) and the square root of $\kappa_c$ multiplied by the surface renewal rate; $\chi$ is the ratio of the dissipation rate by turbulent motion to the total energy dissipation rate; and $V^*$ the wake-to-bubble volume ratio. Equation (14) can be reduced to a dimensionless form as

$$Nu = \frac{A_r}{A_e}\Gamma\chi^{1/4} V^{*-1/4} Re^{3/4} Fr^{-1/4} Pr^{1/2}. \tag{15}$$

Coppus and Rietema presented, in a graphical form, the $\Gamma\chi^{1/4}$ vs $Re$ relation based on experimental results that they themselves and also some other researchers had obtained. We have prepared the following correlations that represent, as demonstrated in Fig. 3, the $\Gamma\chi^{1/4}$ vs $Re$ relation with a reasonable accuracy:

$$\Gamma\chi^{1/4} = 1.2\times10^{-5} Re \qquad (Re \leqslant 6\times10^3) \tag{16a}$$

$$\Gamma\chi^{1/4} = 4\times10^3 Re^{1/3} \qquad (6\times10^3 \leqslant Re \leqslant 2.5\times10^4). \tag{16b}$$

The experimental results of Coppus *et al.* [11] indicate that $V^*$ can well be assumed constant at 22 over the $Re$ range from 70 to 20 000. Substituting the condition that $\theta_w = 50°$ into equation (5) leads to the area ratio $A_r/A_e = 0.763$. Applying these specifications of $\Gamma\chi^{1/4}$, $V^*$ and $A_r/A_e$ to equations (14) and (15), we obtain

$$\alpha_r = 5.54\times10^{-6} Re\,\rho_c c_{pc}\kappa_c^{1/2}(gU/v_c)^{1/4} \qquad (Re \leqslant 6\times10^3) \tag{17a}$$

$$\alpha_r = 1.85\times10^{-3} Re^{1/3}\rho_c c_{pc}\kappa_c^{1/2}(gU/v_c)^{1/4} \qquad (6\times10^3 \leqslant Re \leqslant 2.5\times10^4) \tag{17b}$$

and

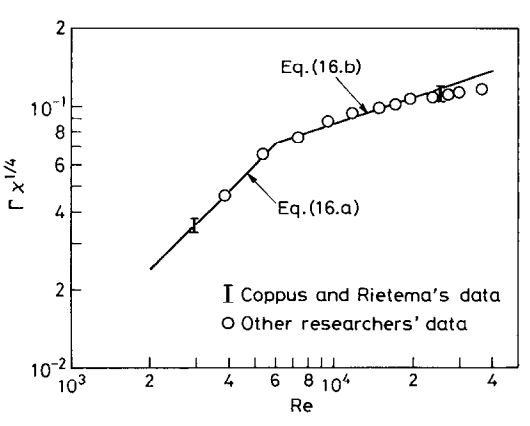


FIG. 3. Curve-fitting correlations for the lead constant, $\Gamma\chi^{1/4}$, in Coppus and Rietema's expression for mass (or heat) transfer coefficient at the rear of a spherical-cap bubble, equation (14).

$$Nu = 4.23 \times 10^{-6} Re^{7/4} Fr^{-1/4} Pr^{1/2} \quad (Re \leqslant 6 \times 10^3) \quad (18a)$$

$$Nu = 1.41 \times 10^{-3} Re^{13/12} Fr^{-1/4} Pr^{1/2} \quad (6 \times 10^3 \leqslant Re \leqslant 2.5 \times 10^4). \quad (18b)$$

Since equations (18a) and (18b) are inadequate to be compared with existing empirical correlations for $Nu$ on a $Nu$–$Re$ diagram, we further simplify the former equations to eliminate $Fr$ from them. This is achieved by introducing the Davies and Taylor equation [12] for the terminal velocity of spherical-cap bubbles

$$U = \frac{2}{3}(gR_c\Delta\rho/\rho_c)^{1/2}. \quad (19)$$

Substituting equation (3) into equation (19) and equating $\theta_w$ to 50°, we obtain

$$U = (0.507gD\Delta\rho/\rho_c)^{1/2}. \quad (20)$$

Since $\Delta\rho/\rho_c \sim 1$ except at very early stages of evaporation, equation (20) is approximated as

$$Fr \equiv U^2/gD = 0.507. \quad (21)$$

Substitution of equation (21) into equations (18a) and (18b) leads to

$$Nu = 5.01 \times 10^{-6} Re^{7/4} Pr^{1/2} \quad (Re \leqslant 6 \times 10^3) \quad (22a)$$

$$Nu = 1.67 \times 10^{-3} Re^{13/12} Pr^{1/2} \quad (6 \times 10^3 \leqslant Re \leqslant 2.5 \times 10^4). \quad (22b)$$

### 3.3. *Comparison of theoretical and experimental results*

The expressions for $Nu$ thus derived are compared with each other and with experimental correlations relevant to the evaporation of relatively large drops. Based on Nazir's experimental data for n-butane drops of $D_0 = 3.5$–$4.0$ mm in water or aqueous sodium chloride solutions under atmospheric pressure [13], Smith [14] provided a correlation of the following form:

$$Nu = 0.072 Re^{0.73} Pr^{1/3}. \quad (23)$$

Another experimental correlation we employ here for reference is one of the correlations that Shimaoka and Mori [6] recently prepared, arranging the data obtained with n-pentane drops of $D_0 = 2.0$–$6.5$ mm in water under pressures of 110–490 kPa; that is

$$Nu = 0.234 Pe^{1/2}. \quad (24)$$

Equations (13), (22a), (22b), (23) and (24) are compared in Fig. 4. It should be remembered that the continuous-phase-side Nusselt number as expressed by each of the former three equations should always be higher than the relevant experimentally-observed Nusselt number which must reflect a finite thermal resistance in each two-phase bubble in addition to the resistance in the continuous phase. Hence it turns out that equation (22a) tends to underestimate $Nu$ with a decrease in $Re$. (Note that this does not necessarily mean that equation (22a) or Coppus and Rietema's surface renewal model inadequately describes the actual heat transfer at the bubble rear, because the underestimation of $Nu$ is possibly ascribable, at least in part, to the neglect of any heat transfer through the bubble front.) We should also note a significant difference between the predictions by equation (13) and those by equations (22a) and (22b). Unfortunately no experimental result is available with which we can evaluate the validities of those predictions and make a discrimination between the two theoretical models. In this context, we are compelled to use both of the models in parallel in the calculation scheme of overall heat transfer coefficient described in the next section.

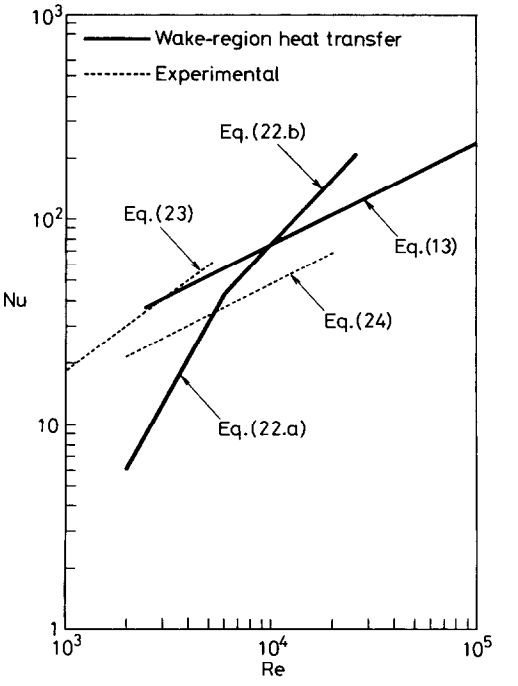


FIG. 4. Comparison of equations (13), (22a) and (22b) with correlations for experimentally-determined Nusselt numbers, equations (23) and (24). Water under pressure of 101.3 kPa and at a temperature of 41.1°C is assumed as the continuous-phase liquid in the graphical plots of these equations. Each graph line extends over a limited $Re$ range in which the relevant equation is self-consistent or based on actual experimental data.

## 4. INTERNAL AND OVERALL HEAT TRANSFER

As mentioned in Section 2, we consider one-dimensional, quasi-steady heat conduction across the layer

of the yet-to-be vaporized liquid supported by the nearly flat base of each bubble. The thickness of the layer may vary from place to place and from time to time. The layer does not necessarily cover all the base area $A_r$. We denote the fraction of $A_r$ 'wetted' by the yet-to-be vaporized liquid by $\zeta$ ($\leqslant 1$). The local thickness of the liquid layer at each instant, $\delta$, is considered to be distributed in a range from 0 to a certain maximum, $\delta_{max}$. We assume that the distribution at any instant through each evaporation process is represented by a simple formula

$$\frac{\delta}{\bar{\delta}_l} = C\cos^m\left(\frac{\pi}{2}s^n\right) \tag{25}$$

where $m = 0$, 2 or 3, and $n = 1$ or 1/2. $\bar{\delta}_l$ designates the liquid layer thickness averaged over the actually 'wetted' area; that is

$$\bar{\delta}_l = V_l/A_r\zeta = \bar{\delta}/\zeta \tag{26}$$

where $\bar{\delta}$ is the liquid layer thickness averaged over the whole area of the bubble base, $A_r$. The variable $s$ means the fraction of the area $A_r\zeta$ wherein the local thickness is larger than, or equal to, a given value of $\delta$. The lead constant $C$ is to be so determined as to satisfy the condition that

$$\int_0^1 \frac{\delta}{\bar{\delta}_l}\mathrm{d}s = 1 \tag{27}$$

and it is specified in Table 1. The class of distributions represented by equation (25) with $n = 1/2$ involves, as a particular (probably the simplest) case, rotationally symmetric distributions expressed as

$$\frac{\delta}{\delta_{max}} = \cos^m\left(\frac{\pi}{2}\frac{r}{r_l}\right) \tag{28}$$

where $\delta_{max}$ is no more than the thickness at the center of the bubble base, $r$ the radial distance from the center, and $r_l$ the radius of the region 'wetted' by the yet-to-be vaporized liquid. The distributions given by equation (25) with the tabulated constants are illustrated in Fig. 5.

Successively we introduce a criterion about $\bar{\delta}_l$. We assume that the yet-to-be vaporized liquid is spread all over the bubble base as long as $\bar{\delta}$ ($= V_l/A_r$) is still larger than, or equal to, a certain critical thickness, $\delta_{cr}$. As $\delta$ decreases below $\delta_{cr}$ in the course of evaporation, dry patches grow on the base, thus reducing $\zeta$ below unity and thereby moderating the decrease in $\bar{\delta}_l$ compared to that in $\bar{\delta}$. The criterion is formulated as

$$\begin{aligned} &\bar{\delta} \geqslant \delta_{cr}; \quad \bar{\delta}_l = \bar{\delta}, \quad \zeta = 1 \\ &\bar{\delta} \leqslant \delta_{cr}; \quad \bar{\delta}_l = \bar{\delta} + \psi(\delta_{cr} - \bar{\delta}), \\ &\qquad\qquad \zeta = \bar{\delta}/\bar{\delta}_l < 1 \end{aligned} \tag{29}$$

where the constant $\psi$ is limited as $0 \leqslant \psi \leqslant 1$.

Table 1. Constants represented by $C$ in equation (25)

| | $m$ | | |
|---|---|---|---|
| | 0 | 2 | 3 |
| $n = 1$ | 1 | 2 | $\frac{3\pi}{4}$ |
| $n = \frac{1}{2}$ | 1 | $\frac{2\pi^2}{\pi^2-4}$ | $\frac{9\pi^2}{2(12\pi-28)}$ |

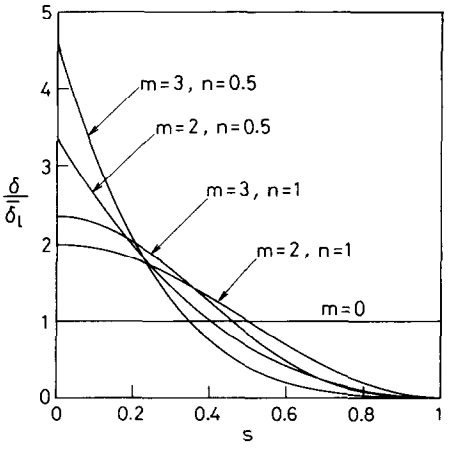


FIG. 5. Assumptions for distribution of the thickness of the yet-to-be vaporized liquid on the base of a spherical-cap bubble.

The overall heat transfer coefficient averaged over the bubble base is given by

$$K = \zeta\int_0^1 \frac{1}{\dfrac{1}{\alpha_r} + \dfrac{\delta}{\lambda_{dl}}}\mathrm{d}s \tag{30}$$

and it is readily converted into the conventionally-defined coefficient, i.e. the overall heat transfer coefficient based on the surface area of a volume-equivalent sphere, as

$$\alpha_{ov} = (A_r/A_e)K \tag{31}$$

where the area ratio $A_r/A_e$ is evaluated by equation (5). Figure 6 shows the predicted variations of $\alpha$ and $\alpha_{ov}$ with the vapor mass fraction $\xi$. Supposed here is the evaporation of an n-pentane drop of $D_0 = 6.2$ mm in a medium of water which is under pressure of 380 kPa and at a temperature in excess of 5 K over the saturation temperature of n-pentane. $U$ and $\alpha_r$ are evaluated by equations (20) and (12), respectively. $\delta_{cr}$ is set at zero. Also shown in Fig. 6 for comparison are the results of three independent experimental runs that are the most relevant, among all of the runs performed in a recent experimental work in our laboratory [6], to the above-mentioned condition. Analogously to the case of spherical bubbles dealt with in ref. [7], an increase in nonuniformity of $\delta$ causes a reduction in the mean internal resistance and hence an increase in $\alpha_{ov}$. The agreement of the predictions

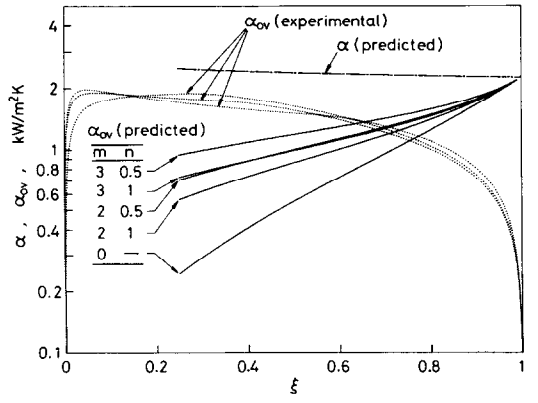


FIG. 6. Predicted variations of overall heat transfer coefficient $\alpha_{ov}$ (solid lines) and continuous-phase-side heat transfer coefficient $\alpha$ ($=(A_r/A_c)\alpha_r$) (chain line) during evaporation of an n-pentane drop in water. $D_0 = 6.2$ mm, $p_\infty = 380$ kPa. $\alpha_r$ is evaluated by equation (12). $\delta_{cr} = 0$. The left-hand end of each graph line corresponds to the condition that $Eo = 40$. Also shown by dotted lines for comparison are experimentally observed variations of $\alpha_{ov}$ for $D_0 = 6.2 \pm 0.2$ mm and $p_\infty = 382 \pm 19$ kPa, which are arranged from the raw data obtained by Shimaoka and Mori [6].

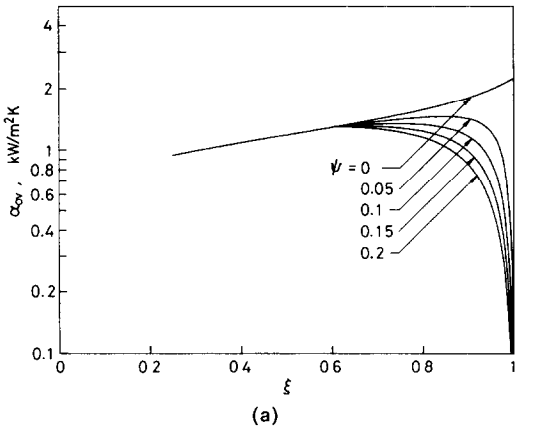


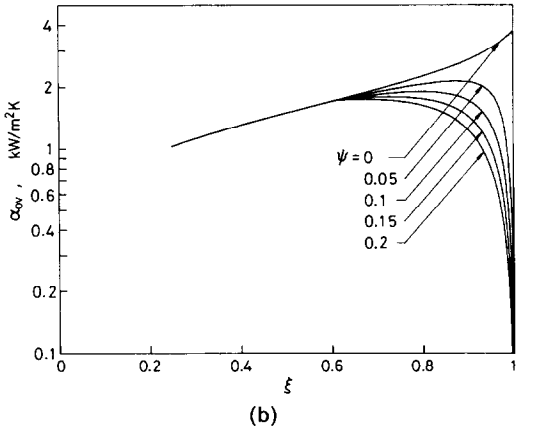


FIG. 7. Predictions of $\alpha_{ov}$ for different specifications for the contraction of the yet-to-be vaporized liquid over the base of a spherical-cap bubble. $m = 3$, $n = 1/2$, $\delta_{cr} = 70$ $\mu$m. $\alpha_r$ is evaluated by equation (12) in (a) and by equations (17a) and (17b) in (b). For other information, consult the caption to Fig. 6.

with relevant experimental results may be said to be better in this case than in the case of spherical bubbles, as far as the magnitudes of $\alpha_{ov}$ in an intermediate range of $\xi$ are concerned. Nevertheless, the predictions fail to simulate the experimentally observed pattern of $\alpha_{ov}$ variation with $\xi$. The sharp drop of $\alpha_{ov}$ at later stages of evaporation, which is recognized in every experimental run, is ascribable to the growth of the 'dry area' on the bubble base, and can be simulated to some extent by substituting some finite value of $\delta_{cr}$ into the calculation procedure. Figure 7 shows the predictions based on the assumption that $\delta_{cr} = 70$ $\mu$m, while $m$ and $n$ are fixed to 3 and 1/2, respectively. In (a) $\alpha_r$ is evaluated by equation (12), while in (b) it is evaluated by equation (17a) or (17b). The latter yields a slightly steeper increase of $\alpha_{ov}$ with $\xi$ whenever $\delta \geqslant \delta_{cr}$. The manner of the drop of $\alpha_{ov}$, with a further increase of $\xi$ resulting in a decrease of $\delta$ below $\delta_{cr}$, is strongly dependent on $\psi$. Upon comparison with the experimental results shown in Fig. 6, $\psi \simeq 0.1$ may be called a rather realistic approximation.

Finally, we compare in Fig. 8 predictions according to the physical model presented in this paper with possibly relevant results obtained by some other researchers through experiments on evaporation of n-butane drops in water or an aqueous solution under the atmospheric pressure. Fortunately, these results are available in the form of correlations that can be used to calculate $\alpha_{ov}$–$\xi$ relations (see Appendix). They are: (a) the time-to-$n$th power expressions ($n$ is an empirical constant) for the heat transferred to, and the distance passed by, each two-phase bubble in each of three particular runs (Nos. 41–43), in Sideman and Taitel's experiments [5], dealing with the largest butane drops ($D_0 = 3.80$–$3.86$ mm) in sea water; (b) the semi-empirical correlation for $\alpha_{ov}$ derived by

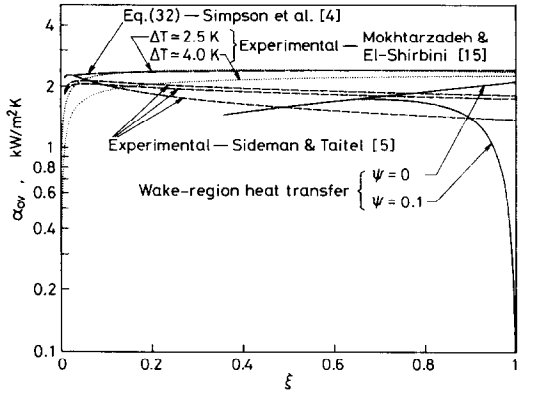


FIG. 8. Variation of $\alpha_{ov}$ during evaporation of an n-butane drop in water or an aqueous solution under atmospheric pressure (101.3 kPa). Compared are the predictions based on the present wake-region heat transfer model for the conditions that $D_0 = 3.8$ mm, $m = 3$, $n = 1/2$, and $\delta_{cr} = 15$ $\mu$m; the results of Runs 41–43, in Sideman and Taitel's experiments [5], that dealt with drops of $D_0 = 3.80$–$3.86$ mm in sea water; equations (32), the semi-empirical correlation by Simpson *et al.* [4]; and Mokhtarzadeh-Dehghan and El-Shirbini's correlations fitted to their data obtained at $\Delta T \simeq 2.5$ and 4.0 K, respectively [15].

Simpson *et al.* [4], which shows excellent agreement with their own experimental data obtained with butane drops of $D_0 = 3.5$–$4.0$ mm in water or in 4 or 8% aqueous sodium chloride solution; and (c) the curve-fitting polynomials prepared by Mokhtarzadeh-Dehghan and El-Shirbini [15] to represent their $\alpha_{ov}$–$D/D_0$ data obtained with butane drops of $D_0 = 3.8$–$4.2$ mm in water at two different levels of the temperature difference $\Delta T$. The correlation of Simpson *et al.* stands on their own theoretical model discussed in Section 1. It is given by

$$\alpha_{ov} = \frac{2.57(D/D_0)^{1/6}}{1+0.206(D/D_0)^{5/12}} \tag{32}$$

where $D/D_0$ is readily related to $\xi$ as indicated by equation (A7) in the Appendix. (Straightforward use of these correlations yields $\alpha_{ov}$ changing only slightly even as $\xi \to 1$. We assume this to be an unreal artifact ascribable to each correlation becoming increasingly inaccurate as $\xi \to 1$.)

In the calculation for drawing the two prediction curves in Fig. 8, we evaluated the properties of butane at its saturation temperature under 101.3 kPa, and those of water at a temperature 5 K higher but under the same pressure. $\alpha_r$ is calculated by use of equation (12). $\delta_{cr}$ is assumed to be 15 $\mu$m, which has no theoretical ground but makes $\alpha_{ov}$ start to decrease, whenever $\psi > 0$, at a seemingly reasonable stage in the later part of each evaporation process.

As already mentioned in Section 1, we readily recognize in Fig. 8 a significant discrepancy between Sideman and Taitel's experimental results and the correlation provided by Simpson *et al.* The former resembles Shimaoka and Mori's experimental results illustrated in Fig. 6 in the pattern of variation of $\alpha_{ov}$ (except at later stages of evaporation), while the latter is in reasonably good agreement with Mokhtarzadeh-Dehghan and El-Shirbini's experimental results. This discrepancy found in the experimental results from different sources cannot be explained at present; it might be ascribed, at least in part, to different data-processing procedures employed in deducing the results. The predictions according to the wake-region heat transfer model approximate the results of Simpson *et al.* and of Mokhtarzadeh-Dehghan and El-Shirbini in the pattern of variation of $\alpha_{ov}$ at intermediate-to-later stages of evaporation, while the predictions are closer to Sideman and Taitel's results in the magnitude of $\alpha_{ov}$ at these stages.

It appears on the whole that the wake-region heat transfer model possibly underestimates $\alpha_{ov}$ at early stages of evaporation but gives rather good predictions of $\alpha_{ov}$ values at intermediate-to-later stages. At early stages of evaporation, the volume of the yet-to-be vaporized liquid is relatively so large that some oscillatory motion of a bubble possibly makes a small fraction of the volume of the liquid periodically climb up the frontal bubble wall over a small distance from the rim of the bubble base. Even a rather short latitudinal distance tentatively wetted by the yet-to-be vaporized liquid may make a significant contribution to the total heat transfer, because of a large azimuthal periphery of a bubble near its rim, an excessively high continuous-phase-side heat transfer coefficient due to a very thin thermal boundary layer developing over the short latitudinal distance above the bubble rim, and a sufficiently small conductive resistance in a thin film of the yet-to-be vaporized liquid spreading over the distance. The underestimation, by the wake-region heat transfer model, of $\alpha_{ov}$ at early stages of evaporation seems to be ascribable to the neglect of possible contribution of such a boundary-layer heat transfer as discussed above. As evaporation progresses, causing a decrease in the volume of the residual liquid in a bubble, the spreading of the liquid will necessarily be limited within the confines of the base of the bubble, thus resulting in a better agreement between the predicted and the experimental values of $\alpha_{ov}$.

## 5. CONCLUDING REMARKS

We have examined for the first time the heat transfer at the rear of a spherical-cap-shaped two-phase bubble forming in the course of direct-contact evaporation of a liquid drop. An analytic model has been constructed, utilizing the penetration or the surface-renewal model to describe the external heat transfer and approximating the internal heat transfer by the heat conduction across the yet-to-be vaporized liquid unevenly distributed on the bubble base. Despite a considerable simplification in describing either heat transfer, the resultant predictions of overall heat transfer are considered reasonable upon comparison with experimental results from a few different sources. The model has of course left considerable room for further refinement, which should be done, in our opinion, in the light of detailed observations, with the aid of some adequate visualization technique, of each evaporating two-phase bubble and its wake. An experimental work in this direction is under way.

*Acknowledgments*—We are indebted to T. Mochizuki and M. Nakayama for their help in the computation, and to H. Shimaoka for preparing the experimental curves shown in Fig. 6 and also for his help in constructing computer programs for deducing some physical properties needed in the present work.

## REFERENCES

1. D. H. Klipstein, Heat transfer to a vaporizing immiscible drop, D.Sc. Thesis, Massachusetts Institute of Technology, Cambridge, Massachusetts (1963).
2. P. P. Wegener and J.-Y. Parlange, Spherical-cap bubbles. In *Annual Review of Fluid Mechanics* (Edited by M. van Dyke, W. G. Vincenti and J. V. Wehausen), Vol. 5, pp. 79–100. Annual Reviews, Palo Alto, California (1973).
3. R. Clift, J. R. Grace and M. E. Weber, *Bubbles, Drops and Particles*, pp. 203–220. Academic Press, New York (1978).
4. H. C. Simpson, G. C. Beggs and M. Nazir, Evaporation

of a droplet of one liquid rising through a second immiscible liquid: a new theory of the heat transfer process, *Proc. 5th Int. Heat Transfer Conf.*, Vol. 5, pp. 59–63. JSME/SCEJ, Tokyo (1974).
5. S. Sideman and Y. Taitel, Direct-contact heat transfer with change of phase: evaporation of drops in an immiscible liquid medium, *Int. J. Heat Mass Transfer* **7**, 1273–1289 (1964).
6. H. Shimaoka and Y. H. Mori, Evaporation of single liquid drops in an immiscible liquid: experiments with n-pentane drops in water and preparation of new heat-transfer correlations, *Exp. Heat Transfer* **3**, 159–172 (1990).
7. Y. H. Mori and N. Ehara, Direct-contact heat transfer to a spherical liquid/vapor two-phase bubble trailing a wake, *Wärme- und Stoffübertr.*, to be published.
8. M. E. Weber, The effect of surface active agents on mass transfer from spherical cap bubbles. *Chem. Engng Sci.* **30**, 1507–1510 (1975).
9. J. T. Lindt and R. G. F. de Groot, The drag on a single bubble accompanied by a periodic wake, *Chem. Engng Sci.* **29**, 957–962 (1974).
10. J. H. C. Coppus and K. Rietema, Mass transfer from spherical cap bubbles: the contribution of the bubble rear, *Trans. Inst. Chem. Engrs* **59**, 54–63 (1981).
11. J. H. C. Coppus, K. Rietema and S. P. P. Ottengraf, Wake phenomena behind spherical-cap bubbles and solid spherical-cap bodies, *Trans. Inst. Chem. Engrs* **55**, 122–129 (1977).
12. R. M. Davies and G. Taylor, The mechanics of large bubbles rising through extended liquids and through liquids in tubes, *Proc. R. Soc. Lond.* **200A**, 375–390 (1950).
13. M. Nazir, Direct-contact heat transfer evaporation of butane drops in brine, Ph.D. Thesis, University of Strathclyde, Glasgow (1972).
14. R. C. Smith, Modeling of fuel-to-steel heat transfer in core disruptive accidents, Ph.D. Thesis, Massachusetts Institute of Technology, Cambridge, Massachusetts (1980).
15. M. R. Mokhtarzadeh-Dehghan and A. A. El-Shirbini, Dynamics of and heat transfer to a butane droplet evaporating in water, *Wärme- und Stoffübertr.* **20**, 69–75 (1986).
16. Y. Shimizu and Y. H. Mori, Evaporation of single liquid drops in an immiscible liquid at elevated pressures: experimental study with n-pentane and R 113 drops in water, *Int. J. Heat Mass Transfer* **31**, 1843–1851 (1988).

## APPENDIX. PREPARATION OF EXPERIMENT-BASED $\alpha_{ov}$–$\xi$ CURVES FOR BUTANE DROP EVAPORATION

As alrcady noted by Mokhtarzadeh-Dehghan and El-Shirbini [15], there exist some inconsistencies in the definition of heat transfer coefficient in the literature dealing with evaporation of butane drops in water or an aqueous solution. We have attempted to eliminate (or to minimize) the inconsistencies, in rearranging the results given in the literature into $\alpha_{ov}$–$\xi$ relations. The inconsistencies and some tricks we have used to eliminate them are specified here to leave no ambiguity concerning the comparison made in Fig. 8.

In Sideman and Taitel's paper [5], the heat transfer coefficient is related to $A$, the instantaneous bubble surface area determined photographically, and to $\Delta T_m$, the arithmetic mean of $\Delta T$ at the top and that at the bottom of their test column. (Note that $\Delta T \equiv T_\infty - T_s$ and, in the extent of the current discussion, $T_s$ is given by the saturation temperature of the dispersed-phase substance corresponding to $p_\infty$.) The surface area thus determined must be larger than $A_e$ to which the data and correlations from the other sources are related. A variable hydrostatic head experienced by each bubble during its ascent may yield a considerable fractional change in $\Delta T$ particularly when $\Delta T_m$ is rather small. Thus, it is not necessarily reasonable to compare the values of the heat transfer coefficient graphically presented in ref. [5] with the results of other previous works as well as with our predictions of $\alpha_{ov}$. Given below is a procedure we used to calculate from Sideman and Taitel's data the $\alpha_{ov}$–$\xi$ relations illustrated in Fig. 8.

Sideman and Taitel presented their data for each experimental run in the form of simple $Q$–$t$, $A$–$t$ and $H$–$t$ correlations, where $t$ is the time lapse after the start of evaporation of a drop, $Q$ the heat transferred to a two-phase bubble evolved from the drop, and $H$ the vertical distance travelled by the bubble. The second correlation is of no use here. $Q$ must have been calculated from $V$, which was measured photographically, assuming that

$$Q = \frac{\rho_{dl}\rho_{dv}}{\rho_{dl}-\rho_{dv}} h_{lv}(V - V_0). \tag{A1}$$

Using equation (A1), we can calculate $A_e$ as

$$A_e = \pi D_0^2 \left(\frac{V}{V_0}\right)^{2/3} = \pi D_0^2 \left[1 + \frac{6}{\pi}\left(1 - \frac{\rho_{dv}}{\rho_{dl}}\right)\frac{Q}{\rho_{dv} h_{lv} D_0^3}\right]^{2/3} \tag{A2}$$

and thereby $\alpha_{ov}$ as

$$\alpha_{ov} = \frac{dQ/dt}{A_e \Delta T} = \frac{dQ/dt}{\pi D_0^2 \left[1 + \frac{6}{\pi}\left(1 - \frac{\rho_{dv}}{\rho_{dl}}\right)\frac{Q}{\rho_{dv} h_{lv} D_0^3}\right]^{2/3} \Delta T}. \tag{A3}$$

The variable temperature difference $\Delta T$ in equation (A3) is estimated on the basis of the Clausius–Clapeyron equation, which can be written, if we assume an instantaneous equilibrium to be established inside a bubble, as

$$dT_s = \left(1 - \frac{\rho_{dv}}{\rho_{dl}}\right)\frac{T_s}{\rho_{dv} h_{lv}} dp_\infty. \tag{A4}$$

Within a relatively small change in $p_\infty$ corresponding to the ascent of a bubble, the $T_s$–$p_\infty$ relation is assumed to be linear with a good approximation. Integrating equation (A4) on this assumption, we obtain

$$T_s - T_{s,m} = \left(1 - \frac{\rho_{dv}}{\rho_{dl}}\right)\frac{\rho_c g(H_m - H)}{\rho_{dv} h_{lv}} T_{s,m} \tag{A5}$$

where $H_m$ is one-half the height of the continuous phase above the location where the evaporation starts, and $T_{s,m}$ means $T_s$ corresponding to $p_\infty$ at $H = H_m$. Equation (A5) is readily rewritten as

$$\Delta T = \Delta T_m - \left(1 - \frac{\rho_{dv}}{\rho_{dl}}\right)\frac{\rho_c g(H_m - H)}{\rho_{dv} h_{lv}} T_{s,m}. \tag{A6}$$

Substituting equation (A6) as well as the $Q$–$t$ and $H$–$t$ correlations into equation (A3), we can calculate $\alpha_{ov}$ varying with $t$. The $Q$–$t$ correlation is also utilized in calculating $\xi$ as the ratio of $Q$ to its final value. Simultaneous calculations of $\alpha_{ov}$ and $\xi$ reveal the $\alpha_{ov}$–$\xi$ relation for the run of interest.

Sideman and Taitel [5] specified neither the salinity concentration in the sea water they used nor the height of the sea water in their test column, $2H_m$, in each run. In the computations to get the $\alpha_{ov}$–$\xi$ relations illustrated in Fig. 8, we assumed that the salinity was 35 wt%, $2H_m = 0.6$ m, and $p_\infty = 101.3$ kPa at the elevation $H = 2H_m$. The difference in the thermal conductivity between pure water and sea water (of about 35 wt% salinity) is less than 1.0% at temperatures of the present interest, and hence the $\alpha_{ov}$–$\xi$ relations thus derived from Sideman and Taitel's data for Runs 41–43 can

be compared, on a common basis, with the other results in Fig. 8.

It seems that the semi-empirical correlation of Simpson *et al.* [4] is consistent with our definition of $\alpha_{ov}$. Before presenting their correlations, Mokhtarzadeh-Dehghan and El-Shirbini [15] clearly stated their definition of $\alpha_{ov}$, which exactly agrees with ours. Thus, we showed in Fig. 8 these correlations as they are, simply applying to them the $D/D_0$-to-$\xi$ conversion

$$\frac{D}{D_0} = \left[1 + \xi\left(\frac{\rho_{dl}}{\rho_{dv}} - 1\right)\right]^{1/3}. \quad \text{(A7)}$$

A remark may be necessary on the possible effect of water-vapor pressure inside bubbles. Shimizu and Mori [16] suggested that $T_s$ should be evaluated as a temperature at which the sum of the vapor pressures of the dispersed-phase substance and the continuous-phase substance, water, equals $p_\infty$. Shimaoka and Mori's experimental results plotted in Fig. 6 as well as equation (24) are based on the above-mentioned evaluation of $T_s$ [6]. It is inconsistent but we have neglected, in deriving equation (A6), the water-vapor pressure; so did Sideman and Taitel [5], Simpson *et al.* [4] and Mokhtarzadeh-Dehghan and El-Shirbini [15]. This inconsistency would have been serious for the evaporation of pentane drops, but is not for the evaporation of butane drops under the atmospheric pressure wherein the water-vapor pressure must be as low as 0.6 kPa or even lower.

## TRANSFERT THERMIQUE DE CONTACT DIRECT LIQUIDE–VAPEUR AU SOMMET SPHERIQUE D'UNE BULLE DIPHASIQUE

**Résumé**—On considère le transfert thermique au sommet sphérique des bulles entre une phase vapeur croissante et un phase liquide qui diminue par vaporisation. La phase liquide est supposée former, dans chaque bulle, une couche inférieure supportée par la base aplatie de la bulle tandis que le reste est occupé par la phase vapeur. Le transfert de chaleur qui cause l'évaporation est supposé opérer à l'arrière de la bulle couverte par le sillage. Les prédictions du transfert thermique global permanent sont comparées avec les résultats expérimentaux correspondants.

## WÄRMEÜBERGANG DURCH DIREKTKONTAKT AN EINE ZWEIPHASIGE BLASE AUS DAMPF UND FLÜSSIGKEIT MIT EINEM KUGELIGEN OBERTEIL

**Zusammenfassung**—Es wird der Wärmeübergang an eine Blase mit kugelförmigem Oberteil betrachtet, die aus einer anwachsenden Dampfphase und einer geringerwerdenden noch zu verdampfenden flüssigen Phase besteht. Es wird angenommen, daß die flüssige Phase den unteren flachen Teil des Volumens einnimmt, während der Rest von der isolierenden Dampfphase ausgefüllt wird. Der Wärmeübergang, welcher die Verdampfung hervorruft, wird daher wohl ausschließlich an der Rückseite der Blase im Nachlaufgebiet auftreten. Der quasistationäre Gesamtwärmeübergang wird berechnet und mit geeigneten Versuchsergebnissen verglichen.

## КОНТАКТНЫЙ ТЕПЛОПЕРЕНОС К ПАРОЖИДКОСТНОМУ ДВУХФАЗНОМУ ПОЛУСФЕРИЧЕСКОМУ ПУЗЫРЬКУ

**Аннотация**—Исследуется теплоперенос к полусферическим пузырькам, каждый из которых состоит из растущей паровой фазы и уменьшающейся, еще не испарившейся жидкой фазы. Предполагается, что в каждом пузырьке жидкая фаза образует нижний слой на плоском основании пузырька, а остальной объем пузырька заполнен теплоизолирующей паровой фазой. Отсюда делается предположение, что вызывающий испарение теплоперенос происходит исключительно в нижней части пузырька. Проводится сравнение расчетов псевдостационарного суммарного теплопереноса с соответствующими экспериментальными данными.